

A modeling of metalized solid fuel surface combustion

SangYeop Han, Jack J. Yoh

Department of Aerospace Engineering, Seoul National University
1 Gwanakro, Gwanakgu, Seoul 08826, South Korea

1 Introduction

Numerical simulation of the combustion process of a metalized pyrotechnic substance is conducted on the mesoscale. Due to many known advantages of solid fuels that burn metal microparticles, metals such as Al, Zr, B, and Mg have been recognized for their high energy density, while these particles behave very differently depending on their particle size, mechanical properties, and chemical reaction characteristics.

Sippel *et al.* investigated the thermal behavior of various types of Al particles such as nano Al, flake Al, spherical Al, and coated Al under the same conditions and visualized the agglomerates of Al particles through the high speed camera imaging [1]. Beckstead [2] presented the models of Al combustion in various environments for aluminized solid rocket propellants. Kim *et al.* conducted numerical analysis on the after burning of a random bed of Al particles induced by detonation of high energetic materials on the mesoscale using level-set method [3,4]. Han *et al.* simulated the behavior of Zr particles in a closed vessel based on the pressure dependent regression rate which assumed a perfectly spherical particle shape [5] as Zr has been widely added in the synthesis of a pyrotechnic initiator.

In the present work, we consider the combustion of non-homogeneous metalized solid fuel on the mesoscale and simulate how metal particles of micron size embedded in a binder behave during the burning process. Figure 1 is a conceptual cartoon illustrating the surface burning of the solid fuel that contains metal particles in a premixed fuel-oxidizer mixture state. In particular, the melt layer where the combustion of metal microparticles takes place is the main domain of focus on the present numerical simulation. The level-set method is used to track the interface of changing particle boundaries and the interaction between the Zr potassium perchlorate (ZPP) particle, a mixture of Zr as fuel and KClO_4 as oxidizer, and binder is considered. The chemical kinetic parameters for the Arrhenius rate law are extracted from the thermochemical analysis using Differential Scanning Calorimetry together with the isoconversional method. The resulting single-step global reaction mechanism is utilized in the numerical simulation for ZPP reaction.

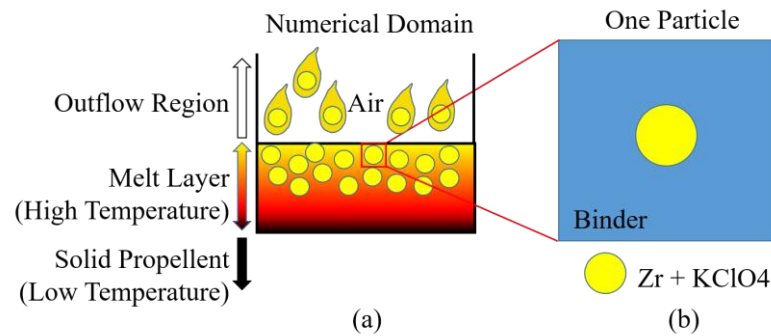


Fig 1. Schematic of surface burning of a metalized solid fuel (zirconium potassium perchlorate, ZPP)

2 Numerical formulation

2.1 Domain separation

ZPP (52wt% Zr, 42wt% KClO_4 , 5wt% Viton B, 1wt% graphite) is used as a representative metalized pyrotechnic substance, subjected to its surface combustion modeling. The oxidizer, KClO_4 , and fuel, Zr, are assumed to be a single mixture and treated separately from the inert binder. The initial shape of this premixed microparticle is assumed to be circular in two dimensions as shown in Fig. 1. A polymeric binder fills the background without additional voids, and the substance above ZPP+Binder is the air.

As the interface between particle and binder is modeled by a level set, one can effectively prescribe the necessary structural behavior of each material such that they deform and vary according to the localized loading pressure. Here, the hot product gas state generated from the particle reaction is calculated in a separate domain as to allow a full gas expansion, not to be bounded by the level set. However, the flow of hot product gas was calculated only in the melt layer and outflow region, and the low temperature solid propellant layer was recognized as a wall in the separate numerical domain. In other words, the numerical domain of the product gas is not the whole but only the melt layer and the outflow region, and the wall boundary condition is applied to the lower part. The boundary between the melt layer representing the condensed phase and the solid propellant layer representing the solid phase is divided based on the melting point of Zr. Hence, the boundary moves as if the chemical reaction proceeds. Effectively, the natural moving boundary condition is imposed on the product gas.

The thermo-chemical properties are inter connected between the two domains of product gas and deforming particles by applying the relevant source terms listed in Eqn. (3). Figure 2 describes the domain separation strategy undertaken, where each boundary condition is summarized in Table 1.

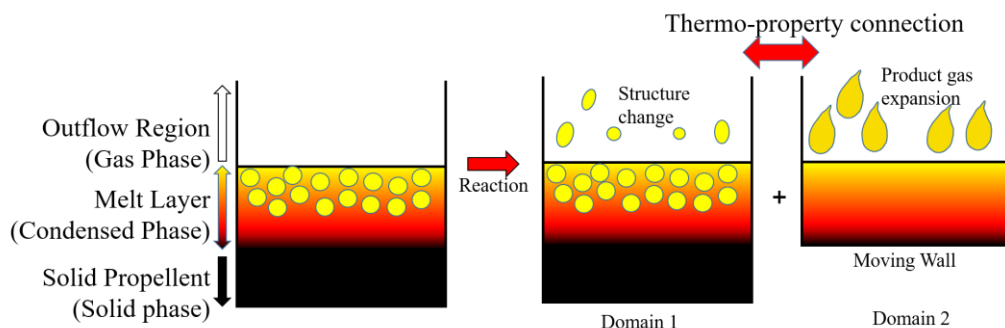


Fig. 2. Schematic of domain separation for the surface burn simulation

Boundary Conditions	Upper	Lower	Left	Right
Domain 1	Zero gradient	Fixed wall (w/o heat transfer)	Periodic	Periodic
Domain 2	Zero gradient	Moving wall (w/o heat transfer)	Periodic	Periodic

Table 1. Boundary conditions

2.2 Governing equations

There are four components considered in the computational domain, namely air, binder, premixed combustible particle, and hot combustion product. Amongst these components, air, binder, and product gas were assumed to be in fluid state having zero strength, while ZPP particles are treated as solid with having strength. Two-dimensional compressible Navier-stokes equations with material strengths are used as shown in Eqns. (1) ~ (3), where strength is turned off for gaseous state.

$$\frac{\partial \vec{U}}{\partial t} + \frac{\partial \vec{E}}{\partial x} + \frac{\partial \vec{F}}{\partial y} = \vec{S}(\vec{U}) + \vec{S}_a(\vec{U}) \quad (1)$$

$$\vec{U} = \begin{bmatrix} \rho \\ \rho u_x \\ \rho u_y \\ \rho E \\ \rho \lambda \\ \rho S_{rr} \\ \rho S_{zz} \\ \rho S_{rz} \end{bmatrix} \quad \vec{E} = \begin{bmatrix} \rho u_x \\ \rho u_x^2 + p \\ \rho u_x u_y \\ u_x(\rho E + p) \\ \rho \lambda u_x \\ \rho S_{xx} u_x \\ \rho S_{yy} u_x \\ \rho S_{xy} u_x \end{bmatrix} \quad \vec{F} = \begin{bmatrix} \rho u_y \\ \rho u_x u_y \\ \rho u_y^2 + p \\ u_y(\rho E + p) \\ \rho \lambda u_y \\ \rho S_{xx} u_y \\ \rho S_{yy} u_y \\ \rho S_{xy} u_y \end{bmatrix} \quad (2)$$

$$\vec{S} = \begin{bmatrix} 0 \\ \frac{\partial S_{xx}}{\partial x} + \frac{\partial S_{xy}}{\partial y} \\ \frac{\partial S_{xy}}{\partial x} + \frac{\partial S_{yy}}{\partial y} \\ \frac{\partial(u_x S_{xx} + u_y S_{xy})}{\partial x} + \frac{\partial(u_x S_{xy} + u_y S_{yy})}{\partial y} + k \left(\frac{\partial^2 T}{\partial x^2} + \frac{\partial^2 T}{\partial y^2} \right) \\ \rho \dot{\lambda} \\ 2S_{xy} \Omega_{xy} + S_{xx} \left(\frac{\partial u_x}{\partial x} + \frac{\partial u_y}{\partial y} \right) + 2G \left(\frac{\partial u_x}{\partial x} - \Sigma - D_{xx}^p \right) \\ -2S_{xy} \Omega_{xy} + S_{yy} \left(\frac{\partial u_x}{\partial x} + \frac{\partial u_y}{\partial y} \right) + 2G \left(\frac{\partial u_y}{\partial y} - \Sigma - D_{yy}^p \right) \\ -\Omega_{xy} (S_{yy} - S_{xx}) + S_{xy} \left(\frac{\partial u_x}{\partial x} + \frac{\partial u_y}{\partial y} \right) + 2G \left(\frac{1}{2} \frac{\partial u_x}{\partial y} + \frac{1}{2} \frac{\partial u_y}{\partial x} - D_{xx}^p \right) \end{bmatrix} \quad \vec{S}_a = \begin{bmatrix} -\rho_{solid} \dot{\lambda} \\ 0 \\ 0 \\ -\rho_{solid} \dot{\lambda} E_{solid} + \rho_{solid} Q \dot{\lambda} \\ 0 \\ 0 \\ 0 \\ 0 \\ 0 \end{bmatrix} \quad \vec{S}_a = \begin{bmatrix} \rho_{solid} \dot{\lambda} \\ 0 \\ 0 \\ \rho_{solid} \dot{\lambda} E_{solid} + \rho_{gas} Q \dot{\lambda} \\ 0 \\ 0 \\ 0 \\ 0 \\ 0 \end{bmatrix} \quad (3)$$

For Solid particle For product gas

As the chemical reaction of solid particle progresses, the solid mass decreases, and product gas of the same mass is generated. In the same way, the total energy of the solid decreases corresponding to the mass converted to the product gas. In addition, the heat of reaction generated as the reaction proceeds is also subsequently considered. All equations are solved by a third-order Runge–Kutta and essentially non-oscillatory (ENO) methods [6] for temporal and spatial discretizations, respectively.

2.3 Equation of state

The equation of state (EOS) for each material is needed for a complete closure to the governing equations. Mie-Grüneisen EOS and Nobel-Abel EOS are used for the unreacted solid ZPP particle and the product gas as shown in Eqns. (4) and (5), respectively. One notes the known versatility of Nobel-Abel EOS for common pyrotechnic product gas as used here [7].

$$p_{\text{particle}} = \Gamma_0 e_0 + \begin{cases} \rho_0 c_0^2 \mu \left[1 + \left(1 - \frac{\Gamma_0}{2} \right) \mu \right] / [1 - (s_0 - 1)\mu]^2 & \text{if } \mu > 0 \\ c_0^2 \rho_0 \mu & \text{if } \mu < 0 \end{cases} \quad (4)$$

$$p_{\text{gas}} = \frac{(\gamma - 1)e}{\nu - b} \quad (5)$$

Here $\mu = \rho/\rho_0 - 1$ and c_0 is speed of sound, s_0 is Hugoniot slope and Γ_0 is Mie-Grüneisen gamma. Coefficient b represents the covolume of the fluid.

3 Results

3.1 Chemical kinetics verification

The constant volume reaction is calculated first before performing the dimensional reaction simulation. Here, the extracted kinetic model is verified by solving the following system of ordinary differential equations for evolutions of temperature and product mass fraction.

$$\rho C \frac{\partial T}{\partial t} = - \frac{\partial \lambda}{\partial t} Q \quad (6)$$

$$\frac{\partial \lambda}{\partial t} = Af(\lambda) \exp\left(\frac{-E_a}{RT}\right) \quad (7)$$

The pre-exponential factor $Af(\lambda)$ and activation energy E_a are functions of λ as obtained from the calorimetry together with the isoconversional method and are shown in Fig. 3. Heat capacity C and measured heat of reaction Q are 536J/kg-K and 2721kJ/kg, respectively.

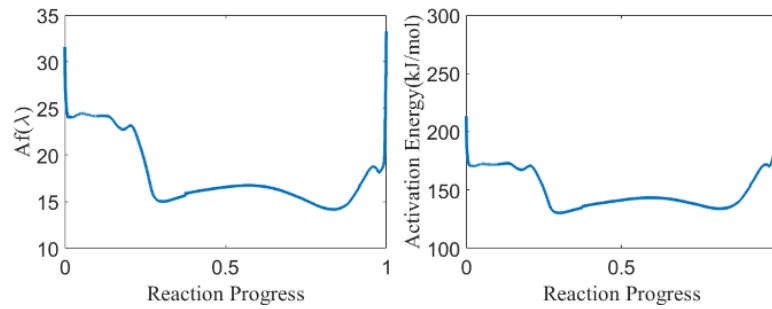


Fig. 3 Arrhenius parameters for ZPP as obtained from the present calorimetric study

Figure 4 shows the calculated reaction progress on the left and temperature history on the right, where the initial temperature is set to 900K for initiation of ZPP reaction.

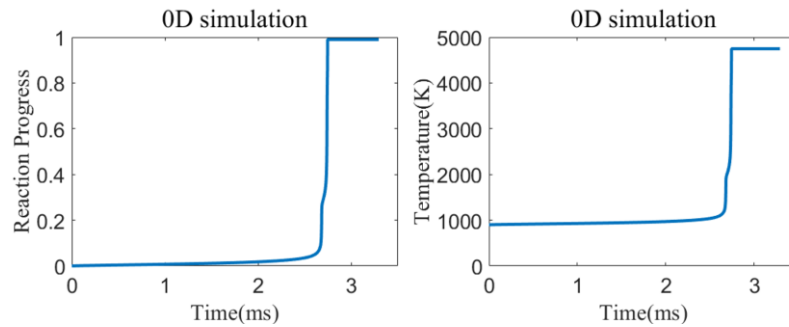


Fig. 4 Simulated reaction progress and temperature evolution for burning ZPP heated at 900K.

Apparently, the burning time for ZPP is about 2.7ms. The reaction occurs rather slowly at the beginning and then exponentially accelerate at about 1500 K.

3.2 Multi-particle reaction

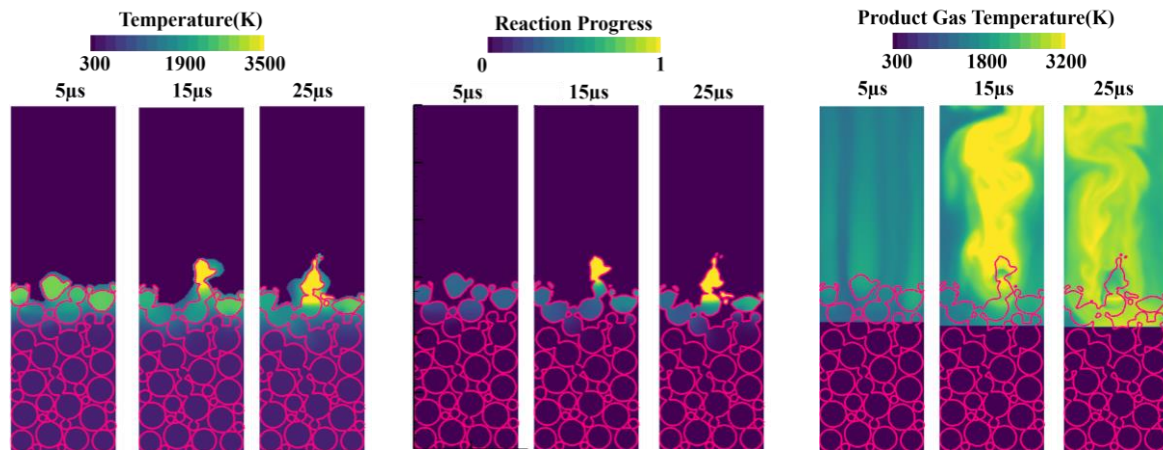


Fig. 5 Simulated evolution of density, reaction progress, and temperature

Figure 5 shows the evolutions of temperature, reaction progress, and product gas temperature for a considered domain of 0.36 mm x 1.2 mm during the early stage of burning. As the reaction proceeds, the particles start to rise upward towards the binder-air interface under the influence of hydrodynamic pressure induced from hot product gas expansion while particle deformations also take place simultaneously. In addition, as the temperature of the condensed phase rises due to the liberation of heat of reaction, the energetic particles in solid state are spontaneously ignited through thermal conduction, and accordingly the boundary between the melt layer and the solid propellant layer is gradually moved downwards. During the chemical reaction, the pressure of the product gas changes significantly, while maintained at approximately 3 MPa near the burning surface. In addition, the temperature of the particles after the reaction was about 3200K, which can vary depending on the distribution of surrounding binder and the degree of accumulation for particles.

3.3 Burning rate comparison

The boundary between the melt layer and the solid propellant layer is considered as the burning surface. It depends on the thermal conductivity of ZPP, chemical reaction rate, structural behavior of solid particles, etc. Table 2 shows the burning rate measurement of ZPP at 3 MPa which is the average pressure around the burning surface. The overall burning rate as calculated in this way is 1400mm/s, which is consistent with the measurement [8].

	Burning rate (mm/s)
This work	$\frac{(0.448 - 0.42) \text{ mm}}{20 \mu\text{s}} = 1400 \text{ mm/s}$
Experiment [8]	$aP^n = 31.51 \text{ mm/s}$ ($a = 19.4 \text{ mm MPa}^{-n}\text{s}^{-1}$, $n = 0.47$)

Table 2. Burning rate comparison

In summary, we have shown some early transient simulation on the surface reaction of a heavily metalized pyrotechnic substance, namely ZPP. The meso-scale modeling of the metal particle reaction is discussed as the product gas is treated separately from the structural issue associated with the deforming particles during the early stage of burning. We expect to present the complete simulation results during the conference.

4. Conclusion

Numerical modeling of melt layer of metalized energetic substance in meso-scale is conducted. Earlier studies have assumed a rigid and perfectly spherical ZPP particle, thus not taking into account the structural changes which always precede well before a full reaction to take place. In essence, we report on the first attempt to simulate both thermal and structural behaviors of multiple metal particles which chemically interact with each other and burn inside the melt layer. The use of level sets embraced by the ghost fluid method framework allowed for smooth interface tracking and for unambiguously defining the interfacial properties extrapolated from the multi-materials.

The findings elucidate that there exists a strong competition between the hydrodynamic pressure induced from the hot product gas generation and the stress field associated with the deforming energetic particles. Thus to accurately model such complex process, the physical burning of the metalized energetic substance at meso-scale must be properly handled.

References

- [1] T.R. Sippel, S.F. Son, L.J. Groven, S. Zhang, E.L. Dreizin (2015), Exploring Mechanisms for Agglomerate Reduction in Composite Solid Propellants with Polyethylene Inclusion Modified Aluminum, *Combustion and Flame* 162 (3) 846-854.
- [2] M.W. Beckstead (2004), A Summary of Aluminum Combustion, Report No.RTO-EN-023, Brigham Young University.
- [3] B.H. Kim, S.H. Choi, J. J. Yoh (2019), Modeling the Shock-induced Multiple Reactions in a Random Bed of Metallic Granules in an Energetic Material, *Combustion and Flame* 210, 54-70.
- [4] S.H. Choi, B.H. Kim, S.Y. Han, J. J. Yoh (2020), Multiscale Modeling of transients in the Shock-induced Detonation of Heterogeneous Energetic Solid Fuels, *Combustion and Flame* 221, 401-415.
- [5] D.H. Han, H.G. Sung, B.Y. Ryu (2017), Numerical Simulation for the Combustion of a Zirconium/Potassium Perchlorate Explosive inside a Closed Vessel, *Propellants, Explosives, Pyrotechnics* 42 (10) 1168-1178.
- [6] B.H. Kim, S.G. Jang, J. J. Yoh (2017), A Full-scale Hydrodynamic Simulation of Energetic Component System, *Computers and Fluids* 156, 368-383.
- [7] A. Chiapolino, R. Saurel (2018), Extended Noble-Abel Stiffened-Gas Equation of State for Sub and Supercritical Liquid-Gas Systems Far from the Critical Point, *Fluids* 3 (3) 48.
- [8] B.L. Poulsen, K.K. Rink (2011), Modeling the Energy Release and Burn Rate Characteristics of ZPP Based Initiators, 49th AIAA Aerospace Sciences Meeting including New Horizons Forum and Aerospace Exposition, AIAA 2011-271